Published in final edited form as:
J Mol Biol. 2008 February 22; 376(3): 705–720. doi:10.1016/j.jmb.2007.11.022.

Structural Biophysics of the NusB:NusE Antitermination Complex

Ranabir Das[1], **Sandra Loss**[1,4], **Jess Li**[1], **David S. Waugh**[2], **Sergey Tarasov**[1], **Paul Wingfield**[3], **R. Andrew Byrd**[1], and **Amanda S. Altieri**[1]

1*Structural Biophysics Laboratory, National Cancer Institute, Frederick, MD,21702*

2*Macromolecular Crystallography Laboratory, National Cancer Institute, Frederick, MD,21702*

3*Protein Expression Laboratory, National Institute of Arthritis and Musculoskeletal and Skin Diseases, National Institutes of Health, Bethesda, MD 20892*

Summary

In prokaryotic transcription regulation several host factors form a complex with RNA polymerase and the nascent mRNA. As part of a process known as antitermination, two of these host factors, NusB and NusE, bind to form a heterodimer, which interacts with a specific *boxA* site on the RNA. The NusB/NusE/boxA RNA ternary complex interacts with the RNA polymerase transcription complex, stabilizing it and allowing transcription past premature termination points. The NusB protein also binds *boxA* RNA individually and retains all specificity for boxA. However, NusE increases the affinity of RNA to NusB in the ternary complex which contributes to efficient antitermination. To understand the molecular mechanism of the process, we have determined the structure of NusB from the thermophilic bacterium *Aquifex aeolicus* and studied the interaction of NusB and NusE. We characterize this binding interaction using NMR, isothermal titration calorimetry, gel-filtration and analytical ultracentrifugation. The binding site of NusE on NusB was determined using NMR chemical shift perturbation studies. We have also determined the NusE binding site in the ternary *E. coli* NusB/NusE/boxA RNA complex and show it is very similar to that in the NusB/NusE complex. There is one loop of residues, from 113−118 in NusB that are affected by NusE binding in the ternary complex, but not in the binary complex. This difference may be correlated to an increase in binding affinity of RNA for the NusB/NusE complex. Funded in part by NCI Contract N01-CO-12400.

Introduction

Antitermination is a critical event for genetic regulation of transcription in both eukaryotic and prokaryotic cells. Antitermination involves the interplay of protein host factors with RNA and the RNA polymerase transcription complex to allow transcription through early termination sites[1]. The transcriptional regulation process in bacteriophage λ can be viewed as a paradigm for antitermination. In phage λ antitermination, the N protein gene product from bacteriophage λ recognizes the nascent mRNA form of the N utilization site (*nut*)[2]. N and several other host proteins, like NusA, NusB, NusE and NusG, associate with *nut* site RNA and the RNA polymerase complex and stabilize transcription for up to several kilobases downstream[1]. The *nut site* is composed of a 12 base single-stranded *boxA* RNA component and a hairpin structured

Correspondence to: R. Andrew Byrd; Amanda S. Altieri.

[4]Present address: Bruker BioSpin AG, Fällanden, Switzerland.

boxB RNA component. The N protein recognizes the *boxB* RNA site and associates with RNA polymerase through NusA. NusG binds to both NusA and RNA polymerase, and can also override defective antitermination inferred by a NusA mutation[3]. The role of NusB is to interact with the *boxA* component of the *nut* site in bacteriophage λ. NusE, another host factor, interacts with NusB[1] and increases the affinity of *boxA* RNA to the complex. NusE also stabilizes the NusB/NusE/RNA ternary complex[4], which presumably associates with RNA polymerase through NusE[1; 5; 6]. However, the mechanism by which NusE enhances the interaction of NusB and *boxA* RNA to facilitate antitermination is not well understood. Insights into these fundamental protein-protein and protein-RNA interactions are applicable to understanding events in both prokaryotic and eukaryotic genetic regulation.

Previous research has indicated that NusB binds to NusE to form a heterodimer, which then binds to *boxA* RNA[4]. A surface plasmon resonance study showed that both *E. coli* (Ec) NusB and co-expressed EcNusB/EcNusE bind to *boxA* RNA, although the co-expressed EcNusB/EcNusE has ten-fold higher affinity towards the RNA[7]. A recent study using fluorescence anisotropy confirms the high affinity of the ternary complex, and also suggests non-specific interactions between NusE and *boxA* RNA in the absence of NusB[8]. In addition, a study of the NusB/NusE complex from *Mycobacterium tuberculosis* (MTb) was reported[9]. These results, which were based on ITC, ultracentrifugation and NMR, indicated binding between MtbNusB and MtbNusE, however the binding site was not identified in that study[9].

The structure has been reported for the *E. Coli*[10], *M. tuberculosis*[11] and *T. maritima*[12] NusB proteins. The NusE protein, also known as ribosomal protein S10, is only partially folded in the absence of the ribosome and has very limited solubility[7; 8]. Our initial attempts to study the EcNusB/EcNusE complex were hindered by the poor solution behavior of EcNusE. Since proteins from thermopiles are often more stable than those from mesophilic bacteria, we explored the NusE protein from *Aquifex aeolicus* (AqNusE). We found AqNusE to be more soluble and better behaved than EcNusE and have determined that the AqNusB and AqNusE proteins also bind to form a heterodimer. Since interaction of NusB/NusE/*boxA* RNA is critical to the antitermination process, studies on the binary and ternary associations are essential to understand the interplay of these host factors. Towards this end, we have characterized the AqNusB and AqNusE proteins using circular dichroism (CD), size-exclusion chromatography and analytical ultracentrifugation. We have determined the solution structure of AqNusB using NMR. We have investigated NusB/NusE binding using isothermal titration calorimetry (ITC) and analytical ultracentrifugation. In addition, we present the binding surface of NusE on NusB determined using NMR chemical shift perturbation for the AqNusB/AqNusE complex and compare it to the NusE binding surface in the ternary EcNusB/EcNusE/*boxA* RNA complex. Detailed investigation of these interactions also provides a viable structural interpretation of modified biological activity in a previously reported protein mutant. Though these interactions are discussed in terms of their role in prokaryotic genetics, the details of protein-protein and protein-RNA interactions may be applicable to eukaryotic genetic regulation as well.

Results

NusB from Aquifex aeolicus

The AqNusB protein contains 148 amino acids (17.1 kDa) and is primarily α-helical, according to its circular dichroism (CD) spectrum which shows a 75% α-helix, 9% β-turn and 15% random coil secondary structure (Figure 1a). AqNusB eluted at 13.8 ml in a gel-filtration study which corresponds to a monomeric NusB protein of 17 (±0.3) kDa (Figure 1b). This result was confirmed by analytical ultracentrifugation (AUC) which observed a molecular weight of 18 (±1) kDa (Figure 1c). AqNusB remains monomeric in solution at concentrations up to 0.7 mM. The ^{1}H, ^{15}N and ^{13}C assignments have been made using standard triple resonance NMR experiments on ^{13}C,^{15}N-labeled AqNusB (see Materials and Methods) and are available at the

BMRB, accession number 15312. Assignments are shown on the ^{1}H-^{15}N HSQC spectrum of AqNusB in Figure 2a. The sequential assignments are 98 % complete: one residue (R2) has no assignments and seven residues (M1, R2, Y3, R4, K139, L145 and S147) have no observable NH resonance due to exchange broadening. The aromatic side chains are completely sequentially assigned. A second minor set of through-bond correlation peaks were noted for residues K134 – S146. AqNusB is 10 residues longer at the C-terminus, as compared to the EcNusB protein sequence, and it is this extension that shows conformational variability.

The solution structure of AqNusB was determined to high resolution using calibrated 3D and 4D NOESY spectra, automated NOESY assignment and structure calculation using the PASD program[13], and subsequent refinement using Xplor-NIH with the addition of $^{1}D_{NH}$ residual dipolar couplings (see Materials and Methods). A summary of restraints and structure quality data are provided in Table 1. The average r.m.s.d. between the backbone atoms of 15 lowest energy structures (residues 3−135) is 0.45 Å (Figure 2b). Structural quality is demonstrated by a low r.m.s.d. of the covalent geometry to ideal values. Evaluation of the backbone torsion angles using Procheck[14] found 99 % of these fall within the allowed regions of the Ramachandran map. The 1% of residues in the disallowed region are found in loops between the helices. The solution structure of AqNusB reveals an all α-helical protein similar in overall fold to known NusB proteins (Figure 3). AqNusB contains seven helices: α_1 (3−20), α_2 (25 −35), α_3 (41−55), α_4 (59−69), α_5 (79−94), α_6 (100−113) and α_7 (117−134). For convenience, the structure can be described as two sub-domains consisting of α1-α3 and α4-α7 that are oriented at an angle of 127° with respect to each other (determined by the angle between the helical axes of α_1 and α_5). This description does not imply motion between helices for any portion of the structure. There are multiple NOE contacts between all helices, including α1 and α5 (see Figure 2 in Reference 10). In addition, the low backbone r.m.s.d. over all helices displayed in Figure 2b, support the stability and lack of flexibility of the NusB structure.

NusE from Aquifex aeolicus

The NusE protein from *A. aeolicus* (AqNusE) contains less ordered structure in solution than the AqNusB protein. The CD spectrum in Figure 4a indicates the secondary structure of NusE contains only 18% α-helix and 30% β-sheet, with the remainder showing 22% β-turn, and 30% random coil. In addition, the ^{1}H-^{15}N HSQC spectrum of AqNusE exhibits an extremely overlapped, broadened spectral region with very few individually distinct peaks (data not shown). These results confirm the paucity of defined secondary structure or globular fold for the AqNusE protein free in solution. The calculated molecular weight of AqNusE from the amino acid sequence is 13.5 kDa. Size exclusion chromatography on a calibrated column shows the molecular weight of AqNusE to be 14 (±1) kDa (Figure 4b). Analysis of the sedimentation equilibrium data for AqNusE gives a molecular mass of 18.0 (±1.1) kDa from a fit to an ideal single species. However, the best fit to the data is obtained when a monomer↔dimer equilibrium model is used with a resulting K_d = 180 (±25) μM (Figure 4c). Indeed, initial AUC data analysis was complicated by the tendency of AqNusE to form higher order aggregates.

AqNusB/AqNusE interaction

The binding interaction between AqNusB and AqNusE was analyzed using ITC, AUC and NMR. The optimal buffer conditions are different for the AqNusB and AqNusE proteins individually, but because the limiting factor in complex formation is low solubility of AqNusE, the AqNusE buffer conditions were used for all experiments on the heterodimer complex (see Materials and Methods for details). The physical characteristics of AqNusB are not affected by the change in buffer conditions, since the CD spectrum is identical and the HSQC spectrum is very similar in either buffer. The interaction between AqNusB and AqNusE was measured using ITC (Figure 5) which shows AqNusB and AqNusE bind to form a heterodimer. From the sign of the heat of the reaction (Figure 5, upper panel) it is apparent that formation of the

AqNusB/AqNusE complex is an endothermic event. The titration curve was fit to a single binding site model and yielded a dissociation constant K_d=1.1 (±0.1) μM with additional parameters N= 1.02 (±0.1), ΔH=12 (±0.02) kcal/mol and ΔS=67.7 (±0.6) cal/(mol deg).

Analytical ultracentrifugation methods were used to analyze the AqNusB interaction with AqNusE in more detail. Initial AUC analysis gives a weight average molecular mass of 50 (±0.6) kDa (Supplemental Figure 1). Analysis of the sedimentation equilibrium data *versus* concentration indicated an increase in molecular mass with concentration (Supplemental Figure 2). From these data, it is clear that the AqNusB:AqNusE heterodimer self-associates to form a 2:2 complex. The sedimentation equilibrium data was then fit to a self-association model, which yields a K_d for $(AqNusB:AqNusE)^2 \leftrightarrow 2(AqNusB:AqNusE)$ of 10 μM (Supplemental Figure 3). A sedimentation velocity experiment was used to see if we could detect the presence of a 1:1 complex. This experiment determines the size of the complex from an estimate of the diffusion coefficient (Supplemental Figure 4, 10 μM complex). From these data, a homogeneous system was observed with a molecular mass of ~ 35 kDa.

Binding site of AqNusE on AqNusB

A chemical shift perturbation study was carried out by NMR, to identify the binding site of AqNusE on AqNusB. At the concentration of the NMR sample (50 μM), the AqNusB:AqNusE complex exists in a 2:2 stoichiometry with a molecular weight of 62 kDa. Thus, per-deuteration of AqNusB was required along with the use of the ^{1}H-^{15}N TROSY-HSQC method[15] in order to obtain a well-resolved spectrum of the NusE-bound AqNusB protein. Chemical shift changes (Δδ) were observed in a subset of the TROSY-HSQC peaks when unlabeled AqNusE is bound, compared to the TROSY-HSQC peaks in the spectrum of free ^{2}H,^{15}N AqNusB (Figure 6a). These Δδ are localized to several places on the surface of AqNusB and are depicted in Figure 6b. Two localized regions of Δδ were found. Residues Y16-E23 comprise the C-terminal end of helix α1 and the loop between helices α1 and α2; and residues S63-E81 include part of helix α4 and the loop between helices α4 and α5. Residues F122, G125, A129, E140 and E141 also show significant Δδ upon NusE binding and are located on helix α7 (Figure 6b).

Binding in the ternary NusB/NusE/RNA E. coli complex

All attempts to form an EcNusB/EcNusE complex in solution resulted in precipitation of the proteins, likely due to the limited solubility of EcNusE beyond ~10 μM. Since the EcNusB/boxA RNA complex is soluble up to 300 μM, we attempted to bind EcNusE to this complex under the assumption that the binding event may keep more EcNusE in solution. A point mutant of EcNusB (C12A) was used in these studies to avoid protein-protein cross-linking from disulfide bond formation between the single, free Cys in EcNusB with the single, free Cys in EcNusE (See Materials and Methods). For simplicity, we will hereafter refer to the C12A EcNusB protein as EcNusB. A sample of ^{2}H,^{15}N–labeled EcNusB was combined with unlabeled boxA RNA at a 1:1.2 ratio, and an HSQC spectrum was collected. For the EcNusB/boxA RNA complex, many HSQC peaks had significant Δδ as compared to the free EcNusB protein[7], indicating possible adjustments in EcNusB to accommodate RNA binding or perhaps a large binding surface. Hence the peaks in the EcNusB/boxA RNA spectrum had to be re-assigned to specific residues using standard backbone triple resonance experiments on a complex of ^{13}C,^{15}N EcNusB/unlabeled boxA RNA[16]. These data and analysis of the EcNusB/boxA RNA complex will be presented elsewhere. This EcNusB/boxA sample was diluted and co-concentrated with EcNusE to 20 μM. The HSQC spectrum of the ternary complex overlaid well with the assigned spectrum of the EcNusB/RNA complex. Several residues exhibited chemical shift differences between EcNusB/RNA in the absence and presence of EcNusE (Figure 7a). The peaks were assigned by nearest peak inspection. The observed Δδ between the spectrum of EcNusB bound to RNA and the spectrum of EcNusB in the EcNusB/EcNusE/RNA ternary complex allow mapping of the binding interface of NusE onto NusB/RNA in this

complex. The chemical shift perturbation data is mapped on the EcNusB solution structure in Figure 7b. The ribbon diagram is given on the left while the surface representation is provided on the right. The residues with less or no chemical shift perturbations are colored blue. From the figure it is seen that significantly perturbed residues include part of the loop between helix α_4 and α_5 (Y61-V80), part of the surface of helix α_7 (G125, V126) and six residues (S113-D118) forming the loop between α_6 and α_7. Residue Y18 of helix α_1 and some nearby residues also show some perturbations when EcNusE binds. A comparison of the chemical shift perturbation data is plotted against the residues for EcNusB (i) and AqNusB (ii) in Figure 7c. The residues along x-axis are aligned according to Altieri et.al[16]. For ease of visual comparison, residues with $\Delta\delta$ beyond the orange line are colored orange in 6b and 7b for the AqNusB and EcNusB structures, respectively. Similarly, the residues with $\Delta\delta$ beyond the yellow and below the orange line are colored yellow in Figure 6b and 7b.

Discussion

Solution Structure of AqNusB

AqNusB was characterized above as a fully folded and monomeric protein in solution by NMR, ultracentrifugation and gel-filtration studies. The high-resolution solution structure of AqNusB (2JR0) shows an all α-helical fold that is very similar to the structures of NusB from *E. Coli*, *M. Tuberculosis* and *T. Maritima*. A superposition of the AqNusB structure to the family of solved NusB structures indicates they are all highly similar (Figures 3b-d). The AqNusB and TmaNusB (1TZT) structures (Figure 3b) match particularly well with a 1.8 Å backbone r.m.s.d. The r.m.s.d. between the EcNusB (1EY1) and AqNusB solution structures is 2.2 Å. Helix α_3 is closer to the core of the protein in AqNusB than it is in EcNusB, giving AqNusB a more compact structure (Figure 3c). The r.m.s.d. between AqNusB and MtbNusB (1EYV) is 2.7 Å over helices α_1 and α_3 - α_7 (Figure 3d). Helix α_2 is further away from α_1 in MtbNusB, which is attributed to the dimer contacts between helix α_2 to α_2' in the MtbNusB crystal structure. Comparison of the various NusB homologue structures indicates a consistently conserved structure, thus implying a consistent molecular interaction mechanism.

Characterization of AqNusE

The inherent insolubility and paucity of defined structural elements we observed for the free EcNusE protein has been noted by others[7; 8] and reported for NusE homologs as well[9]. Despite the increased solubility of the AqNusE homolog over EcNusE, we observe it to be only partly folded in solution based on CD and NMR spectra. As was pointed out in the study of MtbNusE, analysis of the NusE structure as it is found in the crystal of the 30S ribosomal complex from *Thermus thermophilus*[17; 18] provides an explanation of its solution behavior. The ribosome structure shows NusE (identical to ribosomal protein S10 in the complex) to consist of two α-helices from 13−30 and 80−87 and two sections of β-sheet, which involve residues 5−9 and 95−99. In addition, the structure shows a large loop of extended structure from residues 43−69, that is deeply intertwined within the protein-RNA complex. The extended loop and α-helix (13−30) make extensive contacts to the rRNA and the loop also makes hydrophobic contacts with the S3 and S14 proteins[18]. It is likely that these extensive interactions stabilize the NusE structure in the ribosomal complex. The amount of regular secondary structure present in NusE in this complex is consistent with our observed CD results on AqNusE free in solution, and also as reported for NusE homologs[9]. Therefore, it appears that NusE retains its secondary structural elements in the absence of contacts with other proteins or RNA[19], but the area of extended loop conformation in the ribosomal complex is likely disordered in free NusE.

The ultracentrifugation data for AqNusE indicate it does not behave as a single monomeric species in solution, but appreciably self-associates at concentrations above 180 μM. The presence of monomer-dimer equilibria were also reported for MtbNusE in solution[9]. Formation

of the MtbNusE dimer in that study was attributed to a single, free cysteine (C50) in the MtbNusE sequence that would reduce to form an intermolecular disulfide bond. MtbNusE became monomeric in the presence of excess reducing agent or when C50 was mutated to Ser using site-directed mutagenesis[9]. The AqNusE sequence also contains this single cysteine, however, in our case, AqNusE dimerization is not likely due to cysteine cross-linking since our data was run in the presence of excess reducing agent (300 μM TCEP). The C50 residue is not conserved across NusE homologs, therefore, dimerization through this residue is not generally considered important to protein function.

Interaction of NusE and NusB

Isothermal titration calorimetry shows moderate affinity binding between AqNusB and AqNusE with a K_d of ~1 μM. The endothermic nature of the ITC curve corroborates thermodynamic results from the *Mtb*NusB/NusE heterodimer complex[9] and signifies an entropically driven reaction. It is likely, that when the complex forms, there is a loss in entropy from more restricted protein translation and rotation, but there is a larger gain in entropy due to release of ordered water molecules from the interaction surfaces[20; 21; 22]. If binding to NusB also imparts an increase in structure for the disordered regions of NusE, there would be an additional release of water molecules in going from an extended protein chain to a more compact form that would also contribute to the increase in entropy. These results indicate AqNusB/AqNusE binding may be driven by hydrophobic interactions.

Association of the AqNusB:AqNusE heterodimer to form a 2:2 complex is evident from the ultracentrifugation data. This result impacts all biophysical data collected on the AqNusB:AqNusE complex that are above ~10 μM concentration, for which ≥50% will be in the 2:2 form. For the ITC and AUC studies, we have noted the difficulties in obtaining a clear, single species in solution, which is caused by the presence of both heterodimer and “tetramer” in the samples of the complex. During the ITC titration, two binding processes are occurring i)AqNusB binding to AqNusE and ii)self-association of the heterodimer. It is reasonable to assume that the primary binding event is the AqNusB:AqNusE heterodimer formation, since 1) the binding affinity for formation of the heterodimer is ten times greater than that for the tetramer and 2) the first event must proceed to a measurable extent before the second process can take place. The non-ideal appearance of the baseline in the ITC data may very well represent the secondary, tetramerization process. In spite of this complication, our ITC results provide a comparable K_d for the AqNusB/AqNusE interaction (1 μM) to that reported previously for EcNusB:EcNusE (0.2 μM) from fluorescence anisotropy (Reference 8). Because a 1:1 AqNusB/AqNusE complex is observed in the sedimentation velocity experiments, and since the individual proteins do not have a tendency to self-associate at cellular concentrations, we believe the 1:1 heterodimer complex is the physiologically relevant form. The observed self-association at higher (than cellular) concentrations could be caused by a structural adjustment of AqNusB or AqNusE when they bind to each other that then exposes a new binding interface conducive to self-association.

Binding site of AqNusE on AqNusB

NMR studies indicate the binding site of AqNusE on AqNusB. Residues showing significant chemical shift perturbation when AqNusE binds to AqNusB are depicted in Figure 6b. There is a continuous stretch of perturbed residues between S63 and E81. These residues constitute part of helix α_4, and the loop between helices α_4 and α_5. Several residues in this loop are conserved between NusB homologs: I64, I65, H68, L69, W72, I74, D75, L77 and V80. Also, several aliphatic residues on the protein surface formed by this loop create a hydrophobic patch: I64, I65, L69, I74, L77 and V80. Helix α_7 is also highly conserved, and some of the conserved surface residues such as F122, G125, and A129 show significant perturbation upon binding to AqNusE. These residues on α_7 are in structural proximity to the loop formed by residues S63-

E81 in AqNusB, and contribute to the hydrophobic patch formed by the loop. One other significant region of chemical shift perturbation is the loop between helix α_1 and α_2 comprising residues Y16-E23. The surface area formed by these residues is adjacent to the surface at S63-E81. A part of helix α_2 (residues 33−35) also shows chemical shift differences between the bound and free form of AqNusB. Since it is not near the regions described above, these may be secondary shifts due to slight structural adjustment of α_2 as AqNusE interacts with the loop between α_1 and α_2. The chemical shift differences of E140 and E141 at the C-terminus could be accounted for in a similar fashion. The presence of highly conserved NusB residues Y16, L22, D64, L69, L74, L78, V80, F122 and V126 at the binding interface of NusB and NusE, and the fact that the NusE sequence is 94% identical across its homologs[9] suggest that the binding interface would be very similar between the family of NusB and NusE proteins.

NusE binding to NusB/boxA RNA

The role of NusB and NusE in phage λ antitermination also involves their interaction with boxA RNA. The boxA RNA site from different bacteriophages vary somewhat in sequence, as they do even for the leftward (*nutL*) and rightward (*nutR*) transcription directions in phage λ (ref). The antitermination function of NusB in bacterial cells also requires binding to boxA RNA sequences which are present at the rRNA transcription sites. These boxA sequences may differ between each bacterium. To date, the boxA RNA sequence specific for AqNusB has not been found. Nevertheless, we tested whether consensus boxA RNA (3'-CGCUCUUUAACA-5') would bind to the AqNusB protein. Even at an excess of RNA, no shifts were observed in the HSQC spectrum of AqNusB in the presence of consensus boxA RNA. In a similar study, MtbNusB did not bind to consensus boxA RNA *in vitro*[9] and TmaNusB was found to exhibit weak binding to a variant of the boxA sequence[12]. The consensus boxA sequence does, however, bind specifically to EcNusB[7] and the resulting 20 kDa complex is soluble to ~300 μM. Therefore, we utilized the homologous *E. coli* NusB:NusE system (EcNusB:EcNusE) in complex with box A RNA to analyze the binding site of NusE on NusB/RNA.

The binding of EcNusE in the ternary *E. coli* complex was studied by observing differences in the HSQC spectrum between $^{2}H,^{15}N$ EcNusB/boxA RNA and $^{2}H,^{15}N$ EcNusB/boxA/EcNusE (Figure 7a). The observed chemical shift perturbations are mapped onto the free EcNusB structure in Figure 7b. These data show that the loop between residues Y61 and V80 and the intervening region between helices α_4 and α_5 are central to the binding interface. Some residues on the surface of helix α_7 are shifted and contiguous with the Y61-V80 loop: G125 and V126 and possibly F122. A region at the C-terminal end of α_1 (Y18-Q21) is also perturbed. Presented in Figure 7c are a comparison of the chemical shift perturbations (Δδ) observed for AqNusB (i) and EcNusB/RNA (ii) when the respective NusE binds. The shift changes common to the NusE interface in both proteins are the loop between helices α_4 and α_5 (residues 60−81) and the surface residues (G125, K129 and probably F122) of helix α_7. The loop between helices α_1 and α_2 is also perturbed in both complexes, although the region on AqNusB is a few residues longer here. On the other hand, residues S113-D118 are perturbed in EcNusB/RNA with EcNusE but are unperturbed when AqNusB binds AqNusE. Except for these two differences, the NusE binding interface is very similar between the AqNusB/AqNusE and EcNusB/box A/EcNusE complexes. The similarity of the interaction surface of NusB with NusE proteins from two different bacteria emphasize that the NusB/NusE interface, defined here for the first time, is likely to be similar across all NusB and NusE homologs.

As mentioned above, loop residues S113-D118 show large Δδ when EcNusB/RNA interacts with EcNusE (Figures 7a-c). Though the surface of S113-D118 is not very far from the rest of the binding interface (approx 10Å), this region was not perturbed in the AqNusB/AqNusE interaction. It is possible that S113-D118 comes into proximity to the NusE binding interface

by an adjustment of the EcNusB structure when RNA binds. This loop is important both for complex formation and antitermination activity. When EcNusB residue D118 is mutated to Asn in a genetics assay (*nusB101*), this D118N mutant rescues defective antitermination caused by a NusA mutation (*nusA1)* or a NusE mutation (*nusE71*)[23]. This rescue activity requires the presence of *boxA* RNA[23]. Evidently, D118N EcNusB recognizes *boxA* RNA better than wild type EcNusB, which suggests that D118 is part of the contact surface of *boxA* RNA on EcNusB[23]. In support of this hypothesis, D118 shows considerable Δδ between the *boxA* RNA-bound and free EcNusB HSQC spectra[16]. As EcNusE is added to EcNusB/*boxA* RNA complex, the EcNusB D118 HSQC peak shifts further, showing it is additionally affected by binding to EcNusE. In order to affect this, the S113-D118 loop in EcNusB could adjust its position when it binds to RNA such that it is then near the interaction surface of EcNusE. Since the same residue, D118, is affected by interaction of NusB with both factors, NusE and *boxA* RNA are likely to be proximal in the ternary complex. Despite the localized differences in this loop between the binary and ternary complexes, the remaining data indicate the overall binding surface of NusE on NusB is likely similar across all other NusB and NusE homologs. In addition, by comparing Figures 6b and 7b (or Figure 7c) it is apparent that NusE binds to NusB similarly in the absence or presence of boxA RNA.

Biological implications

It is clear that one function of NusE is to increase the affinity of *boxA* RNA for NusB, and it does so by tenfold. The dissociation constant of the NusB and *boxA* RNA interaction is ~2 μM as detected by surface plasmon resonance[7], fluorescence[8] and ITC[16] studies. However, the dissociation constant of boxA for the EcNusB/EcNusE to form NusB/NusE/RNA complex is 200 nM[7; 8]. It is of considerable interest to look for features of the NusB/NusE binary complex that could contribute to formation of the ternary assembly and thus also be important to the function of antitermination.

Presented in Figure 8a and 8b are the electrostatic charge surfaces of the two solution structures of AqNusB and EcNusB, respectively. The surface charge distribution looks similar for the two proteins. In reference to the Figures 8a and 8b, the front surface has a few negatively charged regions, whereas the back surface (not displayed) contains some positively charged patches. Two conserved charged residues, D62 and D75 (or D63 and E75 in EcNusB), are at the NusE binding interface and impart a partial negative charge. These residues may be important contacts to NusE. A previous EcNusE mutant (*nusE71*) that aborts λN mediated transcription antitermination[23; 24] is an alanine to aspartic acid point mutation at position 86 on EcNusE. It is possible that if the hydrophobic A86 of wild type NusE is at the NusB binding surface, the acidic mutation may destabilize the NusB/NusE interaction and cause defective antitermination.

Aromatic residues have been shown to be important in protein-nucleic acid recognition, since aromatic side chains are able to make favorable stacking interactions with nucleic acid bases[25], particularly in the case of non-base paired nucleic acid strands. The NusB family has several conserved aromatic residues in their sequence. Some of these are at or near the surface of the EcNusB structure: Y18, Y69, F114 and F122; while Y16, H68, Y114 and F122, are at the surface of the AqNusB structure. In addition, these conserved aromatic surface residues are affected by NusE binding to NusB in either the binary *A. aeolicus* complex or the *E. coli* ternary complex. These combined observations suggest these aromatic residues, and therefore possibly also NusE, may be close to RNA in the ternary complex. If the *boxA* segment is deleted from the *nut* region (*boxAΔ37*), genetic assays report that antitermination has reduced dependence on NusE[5]. It is also known that free NusE binds RNA non-specifically[8] *in vitro*, and that NusE also has contacts to rRNA in the 30S ribosomal subunit structure[18]. Therefore, NusE may have direct contacts to boxA RNA in the ternary complex. As an indication of where

RNA may interact with NusE, we notice two positively charged regions comprised of residues R43, R45, R46, R66 and K55, H56, K57 that make rRNA contacts with rRNA helices H31, H39 and H41 in the 30S subunit crystal structure. These residues may also have direct contacts with *boxA* RNA in the ternary NusB/NusE/boxA RNA complex and such interactions could significantly increase the stability of the ternary complex.

In Figures 8c-d, the surface representations of AqNusB and EcNusB are drawn with exposed or partially exposed hydrophobic residues colored green. The C-terminus of helix α_4 (S63-L69) and the loop between α_4 and α_5 (L70-E81) are central to the binding interface. AqNusB shows several hydrophobic residues in this region I64, I65, L69, W72, I74, L77 and V80. For this region of EcNusB, residues L62, M66, Y69, L70, L73, L74, L77 and V80 create a hydrophobic surface patch. The presence of a significant number of hydrophobic residues at the NusE interface indicates that hydrophobic interactions could drive the formation of NusB/NusE complex. In a comparison of NusB homolog sequences, a region of highly conserved residues along helix α_7 has been pointed out as possible RNA binding site. As evident in ribbon figures 6b and 7b, the loop 63−80 sits on top of α_7. Due to the loop, some of the conserved hydrophobic residues of α_7, which could be crucial for NusB-RNA interaction, are buried. As indicated by NMR studies, the 63−80 loop undergoes significant chemical shift changes and possible structural adjustment when NusE binds. This structural modification could be enough to expose additional hydrophobic surface area around α_7, and tighten the intermolecular contacts between NusB and RNA.

In conclusion, we have determined the solution structure of AqNusB and studied the AqNusB/AqNusE interaction. Various biophysical methods show that AqNusB is a monomer over a wide range of concentrations, but that AqNusE is exists in a monomer dimer equilibrium with a dissociation constant of ~180 μM. NMR chemical shift mapping provides details of the binding interface on AqNusB when AqNusE is bound. A similar binding region was identified in the *E. coli* system when the EcNusB/RNA complex binds to EcNusE to form the ternary NusB/NusE/RNA complex. Analysis of residues at the interface suggests that NusE binds to NusB largely through hydrophobic interactions. It is also noted that conserved aromatic residues that could be crucial for NusB/RNA interaction, are also perturbed by the NusB/NusE interaction. The present study also shows that D118, which is the site of an important genetic mutation, is also perturbed by the NusB/NusE interaction in presence of RNA. Previous genetic assays[5] and ultracentrifugation studies[8] have shown additional, but non-specific binding between NusE and RNA as well. Hence, that NusB, NusE, and boxA RNA all interact with each other, and the sum of the interactions between the three factors is at a higher affinity than for any of the two factors alone. One possible explanation from evidence gained here is that NusE binding to NusB may induce a modification of loop 63−81 which optimizes contacts between NusB and boxA RNA. With NusB providing the desired specificity to the complex, there is likely a triangular network of interactions between the three factors to enhance the stability of the ternary complex.

Materials and Methods

Cloning, Expression and Purification of AqNusB

The open reading frame (ORF) encoding NusB (AAC06491) was amplified from genomic DNA by the polymerase chain reaction (PCR) using the following oligodeoxyribonucleotide primers: (A) 5'-CCT CCG CAT ATG AGG TAT CGG AAA GGT GCA AG-3' and (B) 5'-TCC CGC GGA TCC ATT ACT CTG ATT TTA AAC TTG GTT TTT CTT C-3'. The resulting PCR amplicon was cleaved with *Nde*I and *Bam*HI and then ligated with the *Nde*I/*Bam*HI vector backbone of pET11c (Novagen, Madison, WI) to create the *A. aeolicus* NusB expression vector pKM772. The nucleotide sequence of the insert was confirmed experimentally. Frozen cells were grown in 1 ml (LBC) at 37 °C for 6 hours. They were then centrifuged and re-suspended

in 50 ml M9 minimal media. (1 L of M9 media contained 1 g $^{15}NH_4Cl$ and 2 g D-$^{13}C_6$-glucose). The cells were incubated for overnight in M9 at 37 °C. The overnight culture was added to 1 L M9 medium and allowed to grow at 37 °C. The protein was induced at an A^{600nm} = 0.8−1.0, using 1 mM IPTG and grown at 37 °C overnight. After centrifugation, the pellet was re-suspended in 30 mM KPO_4. The cells were cracked by sonication and heated to 90 °C for 30 min. They were then centrifuged and the supernatant was applied to a SPsepharose ion-exchange column and eluted with 1 M NaCl in 30 mM KPO_4 phosphate buffer. The purity of the protein was assessed by SDS-PAGE and the relative isotope enrichment was characterized by mass spectroscopy. The isotope enrichment was assessed to be 98% ^{15}N and 98% ^{13}C. To prepare (perdeuterated) ^{2}H-^{15}N labeled AqNusB, the cells were consecutively incubated in 50 ml M9 minimal media in 3 stages. The first contained M9 in 30% D_2O and 70% H_2O, the second containing M9 in 70% D_2O and finally, with M9 in 100% D_2O. (1 L of M9 contained 1g $^{15}NH_4Cl$ and 2g D-^{2}H-$^{12}C_6$-glucose). The rest of the procedure was as described above. The isotope enrichment was assessed to be 98% ^{15}N and 95% ^{2}H (non-exchangeable).

Cloning, Expression and Purification of AqNusE

The ORF encoding *A. aeolicus* NusE (ACC06399) was amplified by PCR using the following oligodeoxyribonucleotide primers: (C) 5'-GGG GAC AAG TTT GTA CAA AAA AGC AGG CTC GGA GAA CCT GTA CTT CCA GGG CAT GGA ACA GGA AAA AAT AAG C-3' and (D) 5'-GGG GAC CAC TTT GTA CAA GAA AGC TGG GTT ATT AAC CTC TCA TCT TCA CTT CTA CGT C-3'. The resulting PCR amplicon was inserted into pDONR201 (Invitrogen, Carlsbad, CA) by Gateway recombinational cloning to create pKM620 and the nucleotide sequence of the insert was confirmed experimentally. Next, the NusE ORF, now with a tobacco etch virus (TEV) protease cleavage site joined in-frame to its N-terminus, was recombined into the maltose-binding protein (MBP) fusion vector pKM596[26] to generate the plasmid expression vector pKM591. The MBP-NusE fusion protein were expressed in *Escherichia coli* BL21(DE3)-RIL CodonPlus cells (Stratagene, Valencia, CA). AqNusE was amplified by PCR based on plasmid pKM620. The PCR 5' primer has an NdeI restriction site at the 5' end, while the 3'primer carries a His_6 sequence followed by a stop codon and a BamHI site. The PCR product was digested by these two enzymes and inserted into pET3a (Novagen) vector. Frozen cells were grown in 1 ml LBC at 37 °C for 6 hours. They were then centrifuged and re-suspended in 100 ml M9 minimal media containing the same amount of $^{14}NH_4Cl$ and D-$^{12}C_6$-glucose as described above. A 1 L culture was grown in M9 overnight. The cells were induced when the A^{600nm} reached 0.8−1.0, with 0.2 mM IPTG at room temperature. These cells were then harvested and re-suspended in 25 ml lysis buffer (50 mM $NaPO_4$, 100 mM NaCl at pH 7.0). A microfluidizer (Microfluidics Corp) was used to crack the cells. After centrifugation, the cell pellet was washed with 50ml lysis buffer and centrifuged again. The pellet was re-suspended in 6 M Gn.HCl, 300 mM NaCL, 50 mM $NaPO_4$, 4 mM DTT buffer at pH 7.0 and 4°C. The resulting combined supernatant was applied to a Ni^{2+} affinity column and eluted with 6 M Gn.HCl, 150 mM imidazole, 300 mM NaCL, 50 mM $NaPO_4$ and 4 mM DTT at pH 7.0. The eluted fractions were pooled together dialyzed in 4M Urea 25 mM KPO_4 and 2 mM DTT at pH 5.5. The protein was refolded by slowly dialyzing away the urea from 4−0 M in the following buffer: 25 mM KPO_4 and 2 mM DTTat pH 5.5. Protein purity was verified by SDS-PAGE and mass spectrometry. For all biophysical experiments, the AqNusE protein was dialyzed into 25 mM KPO4, 100 mM KCl and 300 mM TCEP at pH 5.5.

Expression and Purification of EcNusB and EcNusE

Plasmid construction of C12A EcNusB—Subcloning of the nusB gene into the pET3a vector was achieved by PCR using a pair of oligomers bearing NdeI for the forward oligo and BamHI for the reverse oligo, and using the pNC139 nusB clone (*Court* – reference?), as template. The PCR product was digested with NdeI and BamHI enzymes, and ligated into a pET3a vector. A C12A mutation was introduced into wild type NusB using a pair of

complementary oligomers bearing the mismatch at Cys12 for Ala. Mutagenesis was performed using QuickChange Mutagenesis Kit (Stratagen) using the nusB/pET3a clone.

Protein overexpression and Purification of C12A EcNusB

The pET-3a plasmid containing the nusB mutant sequence (C12A) was used to transform *E. coli* BL21 DE3 (pLysS) cells. ^{15}N-labeled samples were expressed in cells grown on M9 minimal media containing 1 g/L $^{15}NH_4Cl$ and 2 g/L glucose. ^{13}C,^{15}N-labeled samples were expressed in M9 minimal media containing 1 g/L $^{15}NH_4Cl$ and 2 g/L ^{13}C glucose, and in both cases media was supplemented with biotin, thiamine and 100 μg/mL carbenicillin. Cells were grown at 37 °C, induced with 0.5 mM IPTG at $A_{600} \sim 0.8$, harvested 4 h later and frozen at −80 °C. The cells were then defrosted and suspended in 20 mL of buffer containing 300 mM NaCl and 50 mM sodium phosphate (Buffer A). To this cell suspension, 20 μL of RNase at 10 mg/mL concentration, 20 μL of DNase at 10 U/μL concentration and 5 mM $MgSO_4$ were added. The cells were allowed to sit at room temperature for 30 minutes and then centrifuged. The resultant pellet was then washed in Buffer A and centrifuged twice, and was finally dissolved in buffer containing 8M urea, 50mM sodium phosphate at pH 6.8. The sample was then centrifuged to clarity, and the supernatant was loaded onto a HiLoad 26/10 SP Sepharose High Performance cation exchange column (Pharmacia) and purified using a 0−1 M NaCl gradient (in 8 M urea, 50 mM sodium phosphate at pH 6.8). Fractions containing NusB were pooled for refolding by dialysis against decreasing amounts of urea in phosphate buffer at pH 6.8. The refolded protein was run on an SP sepharose column a second time in the same buffer system as described above for the first SP column, except without urea. The purified, refolded protein was then concentrated for NMR to 0.3 mM in100 mM NaCl, 50 mM $NaPO_4$ at pH=6.8. The C12A point mutant of EcNusB was used to avoid protein-protein cross-linking from disulfide bond formation between the single, free Cys in EcNusB with the single, free Cys in EcNusE. The C12 residue is not conserved across the family of NusB homologs, so it is not critical to NusB function. Additionally, the HSQC spectrum of C12A EcNusB is nearly super-imposable with the wild-type EcNusB spectrum and C12A EcNusB maintains wild-type RNA binding.

As a buffer control for the ternary binding data, an identical EcNusB sample was prepared with 10mM urea in the buffer. The HSQC spectrum of EcNusB with and without the urea were identical. The EcNusB/boxA RNA sample was then prepared by adding boxA RNA (3'-UGCUCUUUAACA-5', Oligos Etc, Wilsonville, OR) to ^{2}H,^{15}N-EcNusB and co-concentrating to ~260 μM using an Amicon stirred cell using a 1000 MWCO membrane.

Plasmids of EcNusE were constructed as described earlier[27]. Frozen cells were grown in 1 ml LBC at 37 °C for 6−8 hours till the solution is visibly clouded. The cells were centrifuged and re-suspended in 100 ml M9 minimal media containing $^{14}NH_4Cl$ and D-$^{12}C_6$-glucose. A 1 L culture in M9 was grown at 32°C overnight. Cells were induced when the A_{600nm} reached 0.8 −1.0, with 0.2 mM IPTG and grown for 4hrs at 42°C. These cells were then harvested and re-suspended in 20 ml lysis buffer (50 mM $NaPO_4$, 100 mM NaCl at pH 6.8). A microfluidizer (Microfluidics Corp) was used to crack the cells, and centrifuged. The cell pellet was washed with 50ml lysis buffer and centrifuged again. The pellet was re-suspended in 8M urea, 50 mM $NaPO_4$ buffer at pH 6.8 and swirled overnight at 4°C. The urea lysate was centrifuged to remove insolubles and the supernatant was applied to a SP column and eluted with 8M urea, 50 mM $NaPO_4$, 1 M NaCl at pH 6.8. The eluted fractions were pooled together and diluted with 8M urea, 50 mM $NaPO_4$, 1 M NaCl at pH 6.8. The dilute protein was refolded by a three-step dialysis in these buffers: (i) 4M urea, 50 mM $NaPO_4$, 500 mM NaCl at pH 6.8, (ii) 2M urea, 50 mM $NaPO_4$, 250 mM NaCl at pH 6.8 and (iii) 0 M urea, 50 mM $NaPO_4$, 25 mM NaCl at pH 6.8. Protein purity was verified by SDS-PAGE and mass spectrometry. The ternary

EcNusB/boxA/EcNusB sample for NMR was prepared by diluting the ^{2}H-^{15}N EcNusB/RNA complex and then co-concentrating with EcNusE to 20 μM in the presence of 10mM urea.

Sample preparation of AqNusB

NMR samples of AqNusB were ~0.7 mM prepared in 50 mM phosphate, 200 mM KCl at pH 6.8. All NMR spectra were measured at 35 °C. To measure NH residual dipolar couplings, a 5 %, 5.4 mm diameter polyacrylamide gel was dried and then soaked in an 0.5 mM AqNusB protein solution overnight and finally stretched to 16 mm in length[28]. An NMR sample of ^{2}H,^{15}N-AqNusB complexed with unlabeled AqNusE was prepared by dialyzing the two proteins in 25 mM phosphate, 100 mM KCl, 200 μM TCEP buffer at pH=5.5 and then concentrating to 50 μM. Concentration of the AqNusB/AqNusE complex beyond 100 μM caused aggregation of the sample. All NMR spectra of the heterodimer complex were run at 25 °C.

NMR Spectroscopy and Resonance Assignments

All NMR spectra were collected on 600 and 800 MHz Varian INOVA spectrometers equipped with Nalorac triple resonance gradient probes or Varian cryoprobes. ^{1}H, ^{15}N and ^{13}C backbone resonances were assigned using standard 3D triple resonance NMR experiments: HNCO[29], HNCACB[30] and CBCA(CO) NH[29; 31; 32]. The aliphatic side-chain resonances were assigned from C(CO)NH[33] , H(CCO)NH[34] and HCCH-TOCSY[35] spectra. Aromatic sidechains were assigned from 3D CβHδ, CβHε spectra[36] and a 3D HCCH-aromatic Trosy[15; 37]. All NMR data was processed using NMRPipe[38]. The assignments were derived using ANSIG[39] software.

Backbone ϕ/ψ torsion angle restraints were derived from a database correlating protein secondary structure and ^{13}C chemical shifts using TALOS[40]. One bond residual dipolar couplings (112) were measured from a ^{1}H-^{15}N IPAP-HSQC[41] spectrum of partially aligned AqNusB in a polyacrylamide gel. The NH dipolar couplings ranged from −20.8 to +19.3Hz. The ^{2}H quadrupolar splitting of D_2O in the gel sample was 2.5 Hz. Hydrogen bond restraints were added for residues, whose NHs exhibited slow exchange rates when the lyophilized AqNusB protein was dissolved into D_2O.

Distance information was obtained from the following three- and four- dimensional 13_C and 15N resolved experiments with the given mixing times: 3D ^{15}N NOESY-HSQC (100 ms)[42], 3D ^{13}C NOESY-HSQC (100 ms)[43], 4D ^{13}C/^{15}N HSQC-NOESY-HSQC (100 ms)[44] and 4D ^{13}C/^{13}C HSQC-NOESY-HSQC (100 ms)[45]. The NOESY experiments were peak picked using ANSIG or SPARKY. Possible assignments for NOE each cross peak were then generated within PASD by comparing its chemical shift coordinates to the table of ^{1}H, ^{13}C and ^{15}N backbone and side-chain chemical shift assignments. An error tolerance was allowed in the comparison protocol. The error tolerance was calculated for each NOE spectrum by selecting some unambiguous intra-residue cross-peaks and noting the maximum error between its chemical shift coordinate and its chemical shift assignment. The values for the maximum chemical shift error tolerances for the four NOE spectra were: 0.05 ppm for 1H (F1 and F3), 0.5 ppm for ^{13}C (F2) in the 3D ^{13}C NOESY-HSQC; 0.015 ppm for ^{1}H (F1 and F3), 0.2 ppm for ^{15}N (F2) in the 3D ^{15}N NOESY-HSQC; 1.0 ppm for ^{13}C (F1 and F3), 0.08 ppm for ^{1}H (F2 and F4) in the 4D ^{13}C/^{13}C HSQC-NOESY-HSQC; 0.75 ppm for ^{13}C (F1), 0.08 ppm for ^{1}H (F2 and F4), 0.75 ppm for ^{15}N (F3) in the 4D ^{13}C/^{15}N HSQC-NOESY-HSQC[44] spectrum. The resonances whose chemical shift matched with the coordinates of an NOE cross peak (within tolerance) were assigned to that cross peak. The 4939 NOESY cross-peaks resulted in 112,629 assignments from the chemical shift matching protocol alone, and 438 of these had a single assignment. The intensities of these cross peaks were classified into distance bounds of: 1.8−2.7Å for highest intensity 20% peaks, 1.8−3.3Å for medium intensity 30% peaks, 1.8

−5.0Å for weak intensity 30% peaks, and 1.8−6.0Å for the very weak intensity remaining 20% peaks, and were subsequently used in structure determination.

Structure calculation and refinement

Probabilistic assignment algorithm for Automated Structure Determination or PASD[13] consists of three successive passes of simulated annealing, employing a probabilistic method for the inactivation and reactivation of all NOE assignments on the fly during each pass. The algorithm relies on the observation that a correct set of restraints are correlated and generate forces to determine the same structure, where as incorrect restraints are generally uncorrelated and their forces average out. The simulated annealing passes were set up as detailed in the original paper, at the end of which, 3174 restraints had probability > 0.9 and were included in the final NOE table. At the end of simulated annealing, PASD also provided a high-resolution fold (rmsd = 1.1 between the backbone atoms of the helices over 20 structures) for AqNusB. This initial fold was further refined in XPLOR by 2400 steps of simulated annealing at 400 K followed by 15,000 cooling steps of 0.005 ps to 100 K. In this refinement PASD derived NOEs, observed hydrogen bonds and N-H residual dipolar couplings (Da=−13.2 and Rh=0.67) were used in the list of restraints. The force constants used in the refinement stage of structure calculation were 50 kcal $mole^{-1}Å^{-2}$, 200 kcal $mole^{-1}deg^{-2}$, and 0.1 kcal $mole^{-1}Hz^{-2}$ for NOEs, dihedral angles, and RDCs, respectively.

Size exclusion chromatography—Gel filtration experiments were performed at room temperature using a Tricon 30/100 Superdex75 column with a separation range of 3−70 kDa connected to an FPLC system (AKTA). Absorbance was monitored at 280 nm and 500 μL aliquots samples were analyzed using a flow rate of 0.5 ml/min. The column was calibrated using a standard curve of elution volume versus log of molecular weight made with the following molecular weight standards: ribonuclease (13.7 kDa), chymotrypsinogen A (26 kDa), ovalbumin (43 kDa), and BSA (67 kDa). The AqNusB sample was in 25 mM potassium phosphate and 100 mM KCl buffer at pH 5.5. The AqNusE sample was in an identical buffer with 200 μM TCEP to prevent dimerization through the single free Cys of NusE..

Circular Diochroism spectroscopy—The CD spectra of AqNusB and AqNusE were measured with an Aviv 202 polarimeter. The sample temperature was controlled at 25°C with a Peltier thermostat. The AqNusB sample was in 50 mM potassium phosphate and 200 mM KCl buffer at pH 6.5. The AqNusE sample was in 25 mM potassium phosphate, 100 mM KCl and 200 μM TCEP buffer at pH 5.5. CD spectra were obtained at a protein concentration of about 70 μM using a 1 mm path length quartz cell at 25 °C. The CD spectra shown are single scan measurements.

Isothermal titration calorimetry—Prior to the ITC titration, both proteins were dialyzed separately into a buffer of 25 mM KPO_4, 100 mM KCl and 200 μM TCEP at pH 5.5 The protein binding interactions were measured using a VP- ITC Microcalorimeter (MicroCal LLC, Northampton, MA) at 25 °C. For the titration, 25−27 aliquots (10 μl each) of 100−200 μM AqNusB were injected into the ITC cell containing ~1.4 ml of AqNusE at a concentration of 10 μM. The titration was preceded by a single 2−3 μl injection to eliminate the effect of diffusion at the protein/protein interface at the titration syringe tip during the thermal equilibration of the calorimeter prior to injections. The experiments were run at “Low feedback mode/gain” or at “No feedback” setting. The stirring speed was 300 RPM. The duration of injection in seconds was usually twice the value of injection volume. To offset any thermodynamic effects from dilution of concentrated AqNusB in the syringe, an additional set of injections was run with only buffer in the cell instead of AqNusE. The data from this “blank” experiment were subtracted from the main “protein-into-protein” data. Any dilution effects of AqNusE will be negligible since very small aliquots of AqNusB are used relative to the bulk

volume of the ITC cell. The integrated heat of interaction values were fit using the "Origin 7.0" – based ITC data analysis software provided by MicroCal. There was a small amount of non-ideal behavior noted for each titration point near the baseline, which may be indicative of a secondary thermodynamic process. These were excluded from the fit to the primary binding event by manual adjustment of the integration procedures, as necessary. The initial 2−3 μl titration point was always discarded. The data was fit to the "One set of sites" model which yielded the binding affinity, molar ratio and the other thermodynamic parameters.

Analytical ultracentrifugation—Analytical ultracentrifugation was carried out using a Beckman Optima XL-I analytical ultracentrifuge. Absorption optics, an An-60 Ti rotor and standard double-sector centerpiece cells were used. Equilibrium measurements were made at 20°C and concentration profiles recorded after 16−20 hours at either 18,000 rpm (AqNusB and AqNusE) or 16,550 (AqNusB/AqNusE complex).. Baselines were established by over-speeding at 45,000 rpm for 4 hours. Data (the average of five scans collected using a radial step size of 0.001 cm) were analyzed using the standard Optima XL-I data analysis software. Protein partial specific volumes were calculated from amino acid compositions[46; 47] and solvent density was estimated as previously described[47]. Sedimentation velocity measurements at 20°C were at 45,000 rpm for 3h with data collection at 5−10 minute intervals. Data (radial step size 0.003cm) was analyzed using the program DCDT+ version 2[48]. All of the protein the samples were in 25 mM potassium phosphate and 100 mM KCl at pH 5.5. The AqNusE and AqNusB/AqNusE sample also contained 200 μM TCEP.

Acknowledgement

We thank John Kuszewski and Rob McFeeters for assistance using the PASD program, Marzena Dyba for technical advice, and Karen Routzhan for assistance with the expression and purification protocols for AqNusB and AqNusE. This project has been funded in part by the Intramural Research Program, National Institutes of Health, under contract N01-CO-12400. The content of this publication does not necessarily reflect the views or policies of the Department of Health and Human Services, nor does mention of any trade names, commercial products or organizations imply endorsement by the U.S. Government.

Abbreviations

r.m.s.d, root-mean-square deviation; AqNusB and AqNusE, NusB and NusE proteins from *Aquifex aeolicus*; EcNusB and EcNusE, NusB and NusE proteins from *Escherichia coli*; MtbNusB, NusB protein from *Mycobacterium tuberculosis*; TmaNusB, NusB protein from *Thermatoga maritime*; ITC, isothermal titration calorimetry; CD, Circular Dichroism; AUC, analytical ultracentrifugation..

References

1. Greenblatt J, Nodwell JR, Mason SW. Transcriptional Antitermination. Nature 1993;364:401–406. [PubMed: 8332211]
2. Das, A. How the phage lambda N gene product suppresses transcription termination: communication of RNA polymerase with regulatory proteins mediated by signals in nascent RNA. J. Bacteriol 1992;174:6711–6716. [PubMed: 1400223]
3. Sullivan SL, Ward DF, Gottesman ME. Effect of Escherichia coli nusG function on lambda N-mediated transcription antitermination. J Bacteriol 1992;174:1339–44. [PubMed: 1531224]
4. Greenblatt, J.; McKnight, SL.; Yamamoto, KR., editors. Transcriptional Regulation. Cold Spring Harbor Laboratory Press; New York: 1992.
5. Patterson TA, Zhang Z, Baker T, Johnson LL, Friedman DI, Court DL. Bacteriophage lambda N-dependent transcription antitermination. Competition for an RNA site may regulate antitermination. J. Mol. Biol 1994;236:217–228. [PubMed: 8107107]

6. Mason SW, Greenblatt J. Assembly of transcription elongation complexes containing the N protein of phage lambda and the Escherichia coli elongation factors NusA, NusB, NusG, and S10. Genes Dev 1991;5:1504–1512. [PubMed: 1831176]
7. Luttgen H, Robelek R, Muhlberger R, Diercks T, Schuster SC, Kohler P, Kessler H, Bacher A, Richter G. Transcriptional regulation by antitermination. Interaction of RNA with NusB protein and NusB/NusE protein complex of Escherichia coli. J Mol Biol 2002;316:875–85. [PubMed: 11884128]
8. Greive SJ, Lins AF, von Hippel PH. Assembly of an RNA-protein complex. Binding of NusB and NusE (S10) proteins to boxA RNA nucleates the formation of the antitermination complex involved in controlling rRNA transcription in Escherichia coli. J Biol Chem 2005;280:36397–408. [PubMed: 16109710]
9. Gopal B, Papavinasasundaram KG, Dodson G, Colston MJ, Major SA, Lane AN. Spectroscopic and thermodynamic characterization of the transcription antitermination factor NusE and its interaction with NusB from Mycobacterium tuberculosis. Biochemistry 2001;40:920–8. [PubMed: 11170413]
10. Altieri AS, Mazzulla MJ, Horita DA, Coats RH, Wingfield PT, Das A, Court DL, Byrd RA. The structure of the transcriptional antiterminator NusB from Escherichia coli. Nat Struct Biol 2000;7:470–4. [PubMed: 10881193]
11. Gopal B, Haire LF, Cox RA, Jo Colston M, Major S, Brannigan JA, Smerdon SJ, Dodson G. The crystal structure of NusB from Mycobacterium tuberculosis. Nat Struct Biol 2000;7:475–8. [PubMed: 10881194]
12. Bonin I, Robelek R, Benecke H, Urlaub H, Bacher A, Richter G, Wahl MC. Crystal structures of the antitermination factor NusB from Thermotoga maritima and implications for RNA binding. Biochem J 2004;383:419–28. [PubMed: 15279620]
13. Kuszewski J, Schwieters CD, Garrett DS, Byrd RA, Tjandra N, Clore GM. Completely automated, highly error-tolerant macromolecular structure determination from multidimensional nuclear overhauser enhancement spectra and chemical shift assignments. J Am Chem Soc 2004;126:6258–73. [PubMed: 15149223]
14. Laskowski RA, MacArthur MW, Moss DS, Thornton JM. PROCHECK: A program to check the stereochemical quality of protein structures. J Appl Cryst 1993;26:283–291.
15. Pervushin K, Riek R, Wider G, Wuthrich K. Transverse relaxation-optimized spectroscopy (TROSY) for NMR studies of aromatic spin systems in 13C-labeld proteins. Journal of the American Chemical Society 1998;120:6394–6400.
16. Altieri, AS.; Byrd, RA. Private communication. 2007.
17. Schluenzen F, Tocilj A, Zarivach R, Harms J, Gluehmann M, Janell D, Bashan A, Bartels H, Agmon I, Franceschi F, Yonath A. Structure of functionally activated small ribosomal subunit at 3.3 angstroms resolution. Cell 2000;102:615–23. [PubMed: 11007480]
18. Wimberly BT, Brodersen DE, Clemons WM, Jr. Morgan-Warren RJ, Carter AP, Vonrhein C, Hartsch T, Ramakrishnan V. Structure of the 30S ribosomal subunit. Nature 2000;407:327–39. [PubMed: 11014182]
19. Yaguchi M, Roy C, Wittmann HG. The primary structure of protein S10 from the small ribosomal subunit of Escherichia coli. FEBS Letters 1980;121:113–116. [PubMed: 7007073]
20. Fersht, A. Enzyme structure and mechanism. W. H. Freeman and Company; New York: 1997.
21. Moosavi-Movahedi Z, Safarian S, Zahedi M, Sadeghi M, Saboury AA, Chamani J, Bahrami H, Ashraf-Modarres A, Moosavi-Movahedi AA. Calorimetric and binding dissections of HSA upon interaction with bilirubin. Protein J 2006;25:193–201. [PubMed: 16721655]
22. Wieprecht T, Apostolov O, Beyermann M, Seelig J. Membrane Binding and Pore Formation of the Antibacterial Peptide PGLa: Thermodynamic and Mechanistic Aspects. Biochemistry 2000;39:442–452. [PubMed: 10631006]
23. Court DL, Patterson TA, Baker T, Costantino N, Mao X, Friedman DI. Structural and functional analyses of the transcription-translation proteins NusB and NusE. J. Bacteriol 1995;177:2589–2591. [PubMed: 7730297]
24. Friedman DI, Schauer AT, Baumann MR, Baron LS, Adhya SL. Evidence That Ribosomal Protein-S10 Participates in Control of Transcription Termination. Proceedings of the National Academy of Sciences of the United States of America-Biological Sciences 1981;78:1115–1118.

25. Oubridge C, Ito N, Evans PR, Teo CH, Nagai K. Crystal structure at 1.92 A resolution of the RNA-binding domain of the U1A spliceosomal protein complexed with an RNA hairpin. Nature 1994;372:432–8. [PubMed: 7984237]
26. Fox JD, Waugh DS. Maltose-binding protein as a solubility enhancer. Methods Mol Biol 2003;205:99–117. [PubMed: 12491882]
27. Das A, Pal M, Mena JG, Whalen W, Wolska K, Crossley R, Rees W, von Hippel PH, Costantino N, Court D, Mazzulla M, Altieri AS, Byrd RA, Chattopadhyay S, DeVito J, Ghosh B. Components of multiprotein-RNA complex that controls transcription elongation in Escherichia coli phage lambda. Methods Enzymol 1996;274:374–402. [PubMed: 8902820]
28. Bax A, Kontaxis G, Tjandra N. Dipolar couplings in macromolecular structure determination. Methods Enzymol 2001;339:127–74. [PubMed: 11462810]
29. Grzesiek S, Bax A. Improved 3D triple-resonance NMR techniques applied to a 31kDa protein. Journal of Magnetic Resonance 1992;96:432–440.
30. Wittekind M, Mueller L. HNCACB, a high-sensitivity 3D NMR experiment to correlate amide-proton and nitrogen resonances with the alpha- and beta-carbon resonances in proteins. Journal of Magnetic Resonance, Series B 1993;101:201–205.
31. Muhandiram DR, Kay LE. Gradient-enhanced triple-resonance three-dimensional NMR experiments with improved sensitivity. Journal of Magnetic Resonance, Series B 1994;103:203–216.
32. Kay LE. Field gradient techniques in NMR spectroscopy. Current Biology 1995;5:674–681.
33. Grzesiek S, Bax A. Correlating backbone amide and side chain resonances in larger proteins by multiple relayed triple resonance NMR. Journal of the American Chemical Society 1992;114:6291–6293.
34. Montelione GT, Lyons BA, Emerson SD, Tashiro M. An efficient triple resonance experiment using carbon-13 isotropic mixing for determining sequence-specific resonance assignments of isotopically-enriched proteins. J Am Chem Soc 1992;114:10974.
35. Kay LE, Xu GY, Singer AU, Muhandiram DR, Forman-Kay JD. A gradient-enhanced HCCH-TOCSY experiment for recording side-chain ^{1}H and ^{13}C correlations in H{-2}O samples of proteins. Journal of Magnetic Resonance, Series B 1993;101:333–337.
36. Yamazaki T, Forman-Kay, JD, Kay LE. Two-dimensional NMR experiments for correlating $^{13}C^{\beta}$ and $^{1}H^{\delta/\varepsilon}$ chemical shifts of aromatic residues in ^{13}C-labeled proteins via scalar couplings. Journal of the American Chemical Society 1993;115:11054–11055.
37. Meissner A, Sorensen OW. Suppression of diagonal peaks in three-dimensional protein NMR TROSY-type HCCH correlation experiments. J Magn Reson 2000;144:171–4. [PubMed: 10783289]
38. Delaglio F, Grzesiek S, Vuister GW, Zhu G, Pfeifer J, Bax A. NMRPipe: a multidimensional spectral processing system based on UNIX pipes. J Biomol NMR 1995;6:277–293. [PubMed: 8520220]
39. Kraulis J, Clore GM, Nilges M, Jones TA, Pettersson G, Knowles J, Gronenborn AM. Determination of the three-dimensional solution structure of the C- terminal domain of cellobiohydrolase I from Trichoderma reesei. A study using nuclear magnetic resonance and hybrid distance geometry-dynamical simulated annealing. Biochemistry 1989;28:7241–7257. [PubMed: 2554967]
40. Cornilescu G, Delaglio F, Bax A. Protein backbone angle restraints from searching a database for chemical shift and sequence homology. J Biomol NMR 1999;13:289–302. [PubMed: 10212987]
41. Ottiger M, Delaglio F, Bax A. Measurement of J and dipolar couplings from simplified two-dimensional NMR spectra. J Magn Reson 1998;131:373–8. [PubMed: 9571116]
42. Zhang O, Kay LE, Olivier JP, Forman-Kay JD. Backbone 1H and 15N resonance assignments of the N-terminal SH3 domain of drk in folded and unfolded states using enhanced-sensitivity pulsed field gradient NMR techniques. J Biomol NMR 1994;4:845–58. [PubMed: 7812156]
43. Muhandiram DR, Farrow NA, Xu G-Y, Smallcombe SH, Kay LE. A gradient 13C NOESY-HSQC experiment for recording NOESY spectra of 13C-labeled proteins dissolved in H2O. Journal of Magnetic Resonance, Series B 1993;102:317–321.
44. Kay LE, Clore GM, Bax A, Gronenborn AM. Four-dimensional heteronuclear triple-resonance NMR spectroscopy of interleukin-1 beta in solution. Science 1990;249:411–414. [PubMed: 2377896]
45. Zuiderweg ERP, Petros AM, Fesik S, Olejniczak ET. Four-dimensional [13C,1H,13C,1H] HMQC-NOE-HMQC NMR spectroscopy: Resolving tertiary NOE distance constraints in the spectra of larger proteins. Journal of the American Chemical Society 1991;113:370–372.

46. Cohn, EJ.; Edsall, JT. Proteins, Amino Acids and Peptides. Van Nostrand-Reinhold; Princeton, NJ: 1943.

47. Laue, TM.; Shah, BD.; Ridgeway, TM.; Pelletier, SL. Analytical Ultracentrifugation in Biochemistry and Polymer Science. Harding, SE.; Rowe, AJ.; Horton, JC., editors. Royal Society for Chemistry; 1992.

48. Philo JS. Improved methods for fitting sedimentation coefficient distributions derived by time-derivative techniques. Anal Biochem 2006;354:238–46. [PubMed: 16730633]

49. Guex N, Peitsch MC. SWISS-MODEL and the Swiss-PdbViewer: an environment for comparative protein modeling. Electrophoresis 1997;18:2714–23. [PubMed: 9504803]

Supplementary Material

Refer to Web version on PubMed Central for supplementary material.

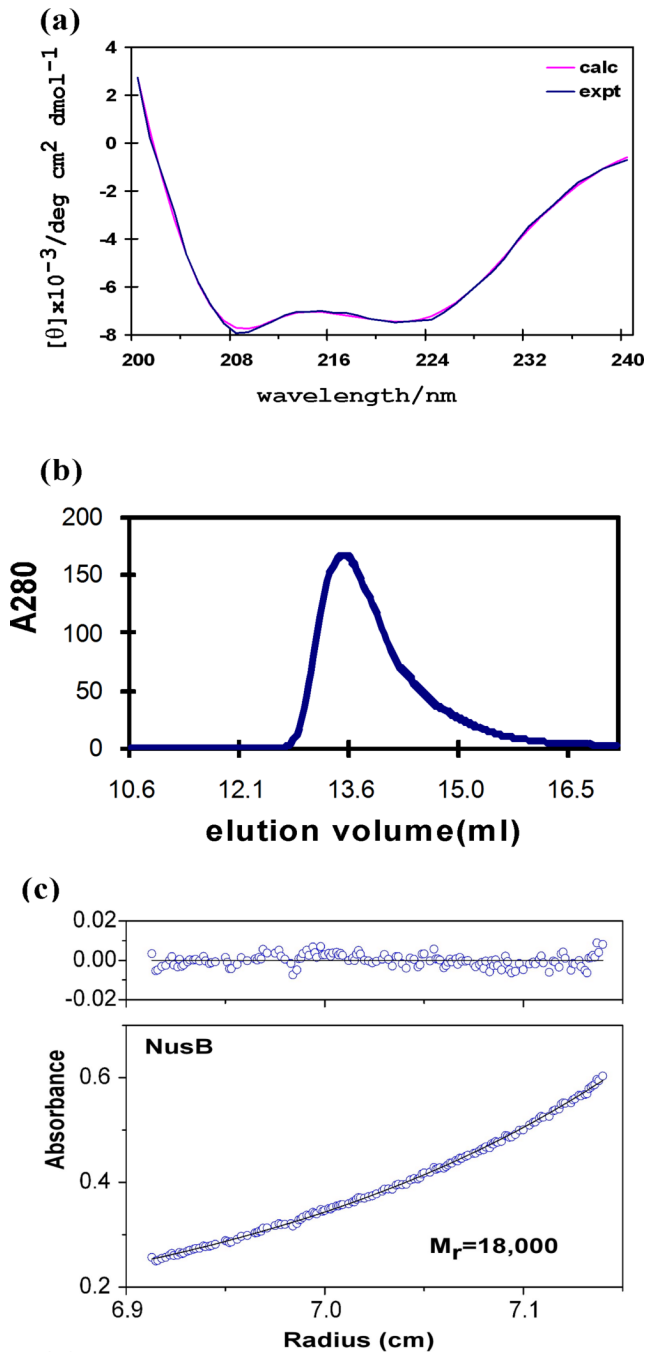

Figure 1.

Characterization of AqNusB. (a) Far UV-CD spectra. The data is drawn in blue and the calculated curve from the CONTIN algorithm is drawn in pink. (b) gel-filtration of AqNusB shows the protein elutes at 13.8 ml corresponding to 17 kDa (expected 17 kDa). (c)Analytical ultracentrifugation results on AqNusB yielded a molecular weight of 18 kDa at 100 μM protein concentration.

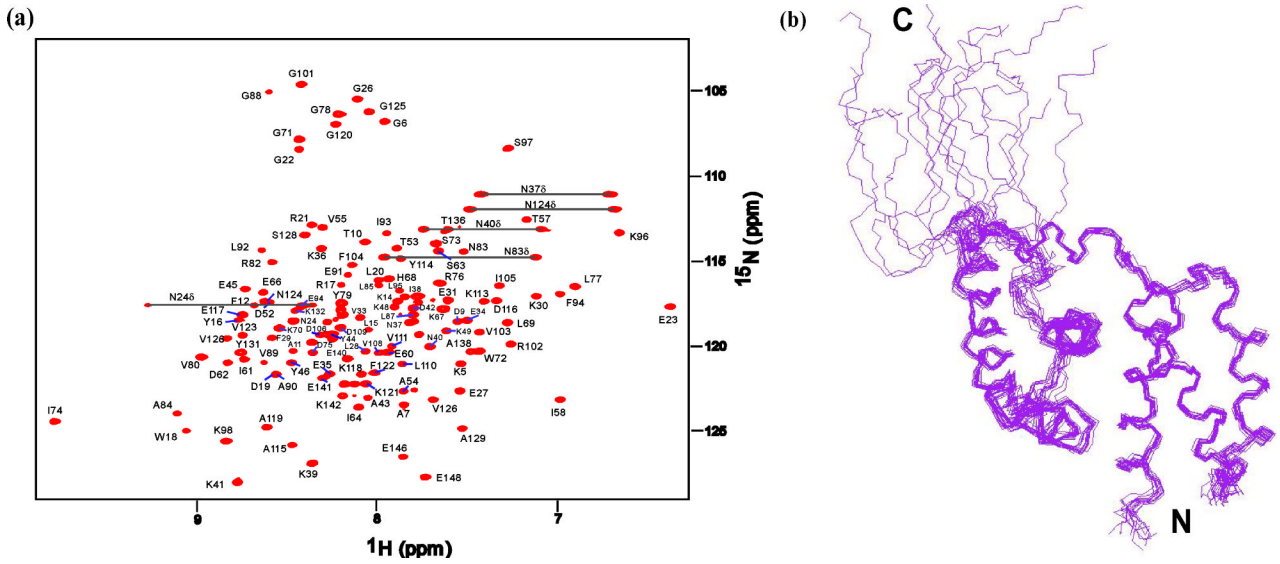

Figure 2.

Solution NMR spectrum and structure of AqNusB. (a) Sequentially assigned HSQC spectrum of (perdeuterated) ^{2}H, ^{15}N AqNusB. (b) Ensemble of the 15 lowest energy solution structures calculated using the PASD algorithm followed by simulated annealing refinement which included *112* $^{1}D_{NH}$ residual dipolar couplings.

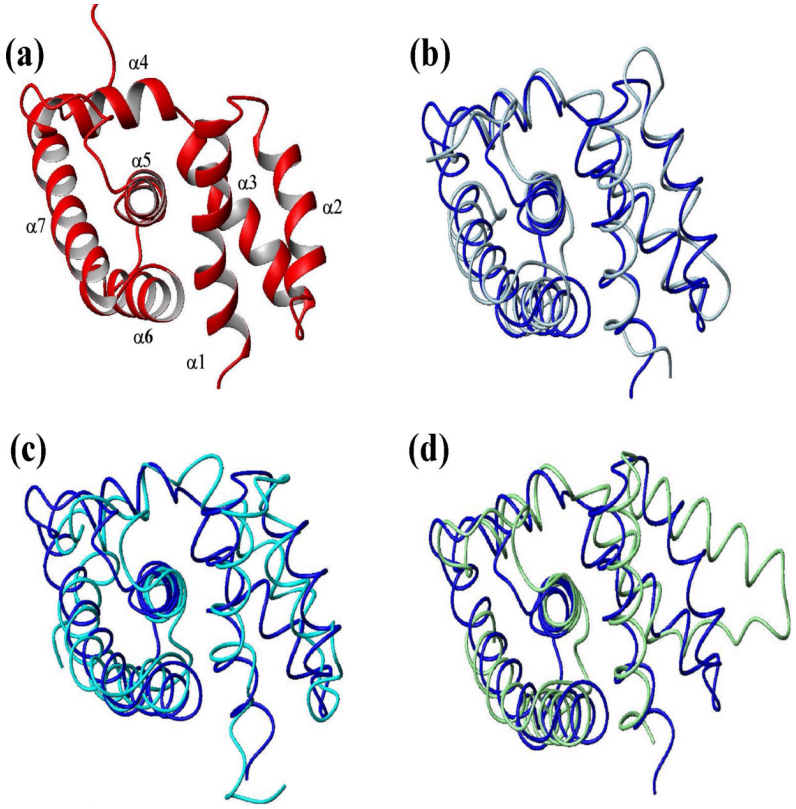

Figure 3.
Comparison of NusB homologous structures. (a) Ribbon trace of AqNusB solution structure. Comparison of AqNusB (blue) to (b) TmaNusB (silver), (c) EcNusB (cyan), and (d) MtbNusB (green).

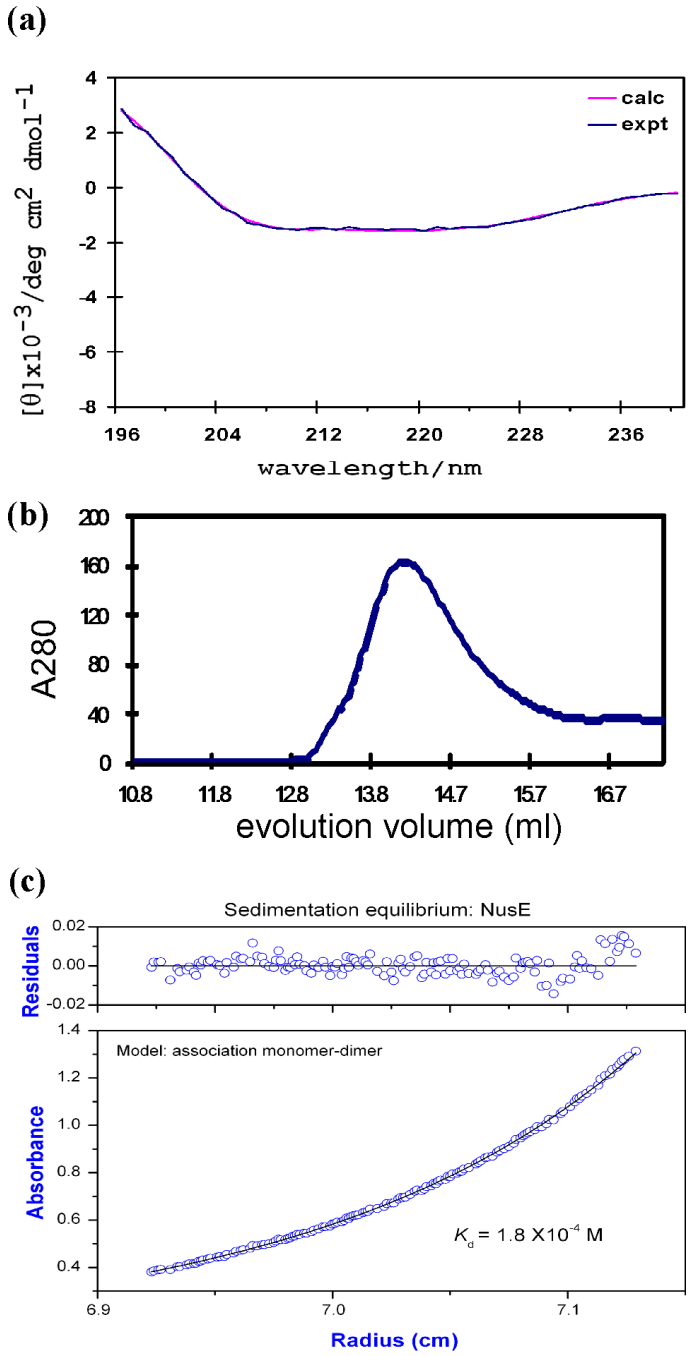

Figure 4.

Characterization of AqNusE. (a) Far UV-CD spectra. The experimental data is drawn in blue and the curve fit from the CONTIN algorithm is drawn in pink. (b)Size exclusion data of AqNusE at 5 μM. AqNusE elutes at 14.6 ml corresponding to 14(±1) kDa using a calibrated curve (see Materials and Methods). The expected molecular weight from the amino acid sequence is 13.5 kDa. A dilution factor of 1.5−2 was taken into consideration for the column. (c) Sedimentation equilibrium results for a 50 μM sample of AqNusE yields a molecular weight of 18 (±1.1) kDa. The data fit best to a monomer↔dimer model with a resulting K_d = 180 (±25) μM.

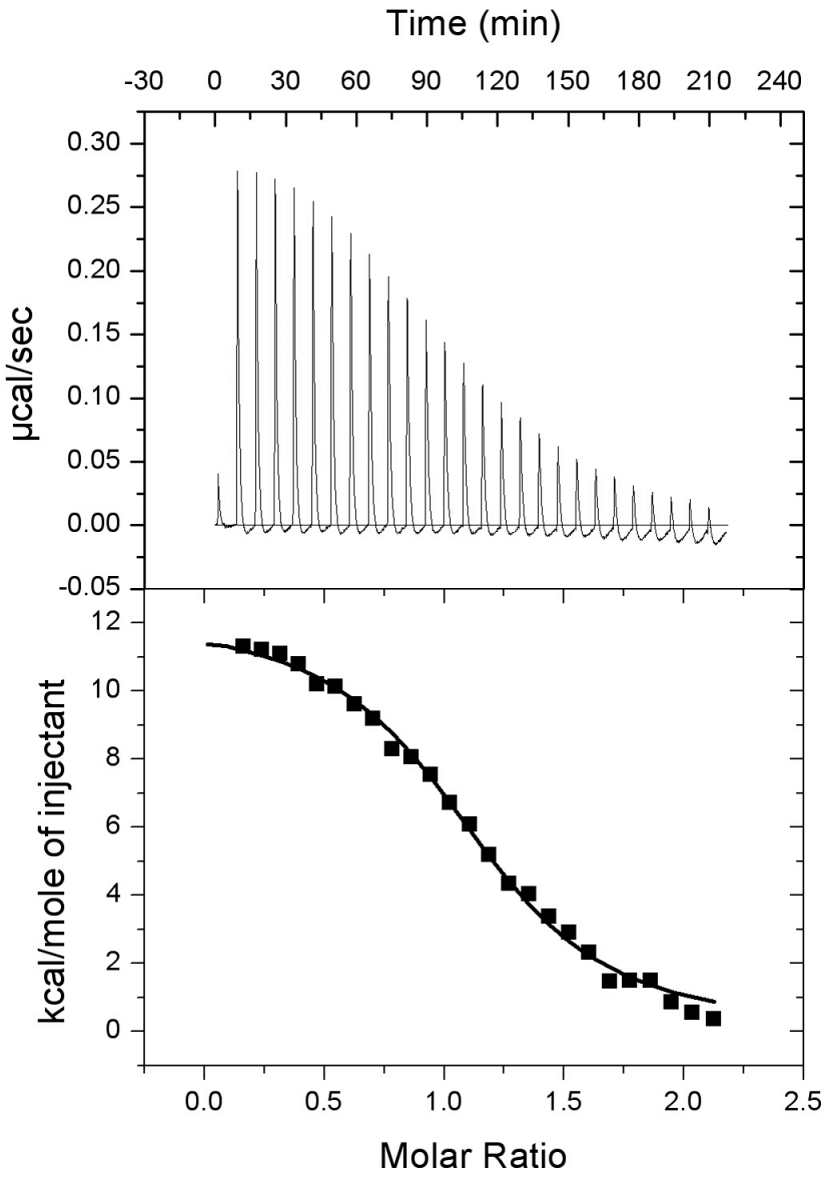

Figure 5.
Interaction between NusB and NusE observed by isothermal titration calorimetry. ITC data is from 150 μM NusB titrated into 10 μM NusE. The titration curve indicates an endothermic reaction with a dissociation constant K_d = 1μM.

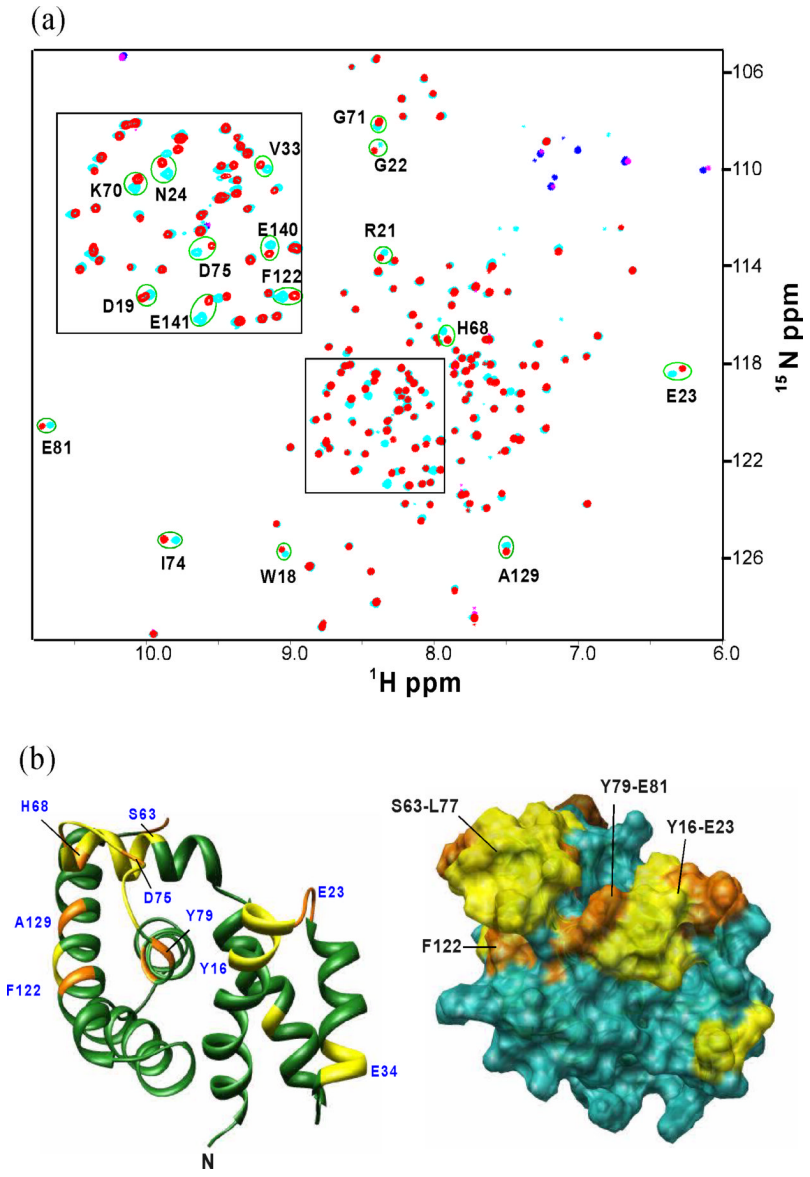

Figure 6.

Chemical shift perturbation of AqNusB by AqNusE. (a) Comparison of TROSY-HSQC spectrum of ^{15}N, ^{2}H-labeled AqNusB when it is free (cyan) and in complex with unlabeled AqNusE (red). Folded peaks from Arginine side chains appear in blue in the free form and magenta in the complex spectrum, respectively. (b) Mapping of AqNusB residues showing significant chemical shifts when NusE binds. The C-terminal residues 142−148 are unaffected by NusE and are not displayed for clarity. Residues showing $\Delta\delta > 0.4$ ppm are colored orange, <0.2 ppm $\Delta\delta < 0.4$ ppm are colored yellow, while $\Delta\delta < 0.2$ ppm are colored dark green. Some significant perturbed residues are numbered in blue. The surface representation is similar except that the $\Delta\delta < 0.2$ ppm residues are colored in sea-green. The shift mapping indicates two sites with significant shifts at the residues 63−81 and 18−23.

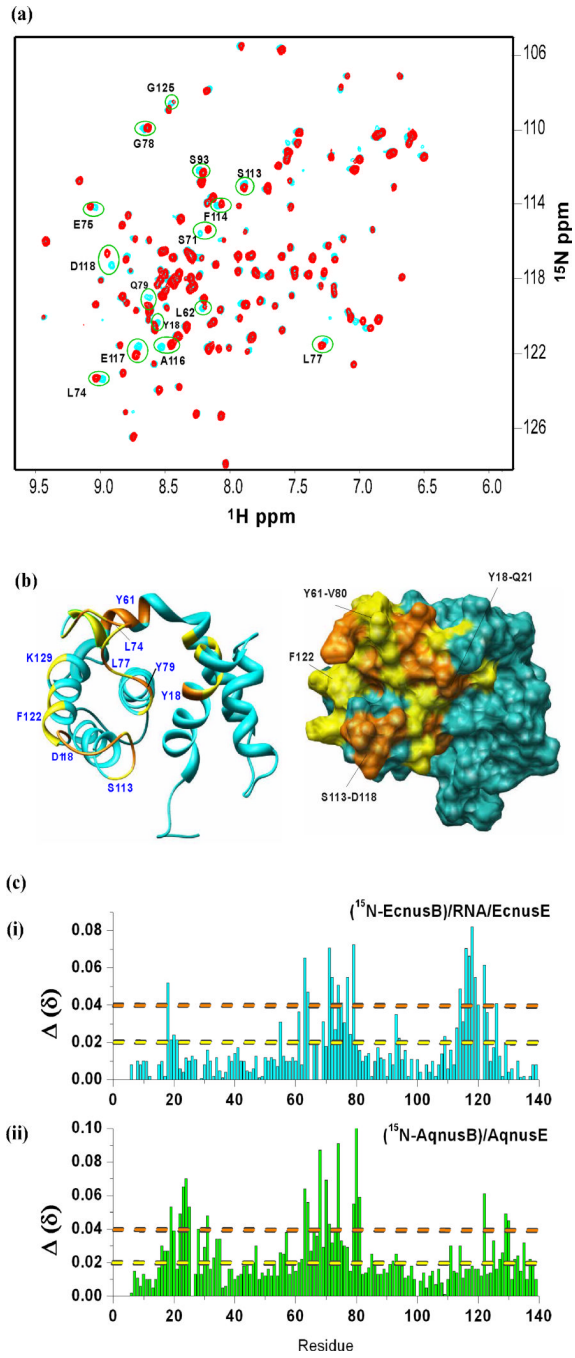

Figure 7.

Chemical shift perturbation of EcNusB in the EcNusB/EcNusE/RNA complex studied by NMR. (a) Comparison of HSQC spectrum of, $^{2}H,^{15}N$-labeled EcNusB when it is bound to *boxA* RNA (cyan), and when it is in the ternary complex with unlabeled EcNusE and *boxA* RNA (red). (b) Mapping the significant chemical shifts on the structure of EcNusB (PDB ID: 1EY1). Residues with $\Delta\delta > 0.4$ ppm are labeled orange, <0.2 ppm $\Delta\delta < 0.4$ ppm are labeled yellow, while $\Delta\delta < 0.2$ ppm are labeled cyan. Some of the significantly shifted residues are numbered in blue. The surface representation is similar except that the $\Delta\delta < 0.2$ ppm residues are colored in light-blue. The mapping indicates two sites with significant shifts at the residues

63−79 and 18−21. (c) A graph of the chemical shift $\Delta\delta = ((\Delta\delta)^2+(\Delta N/5)^2)^{1/2}$ *versus* residue number for *E. coli* (red) and *Aquifex* NusB (green).

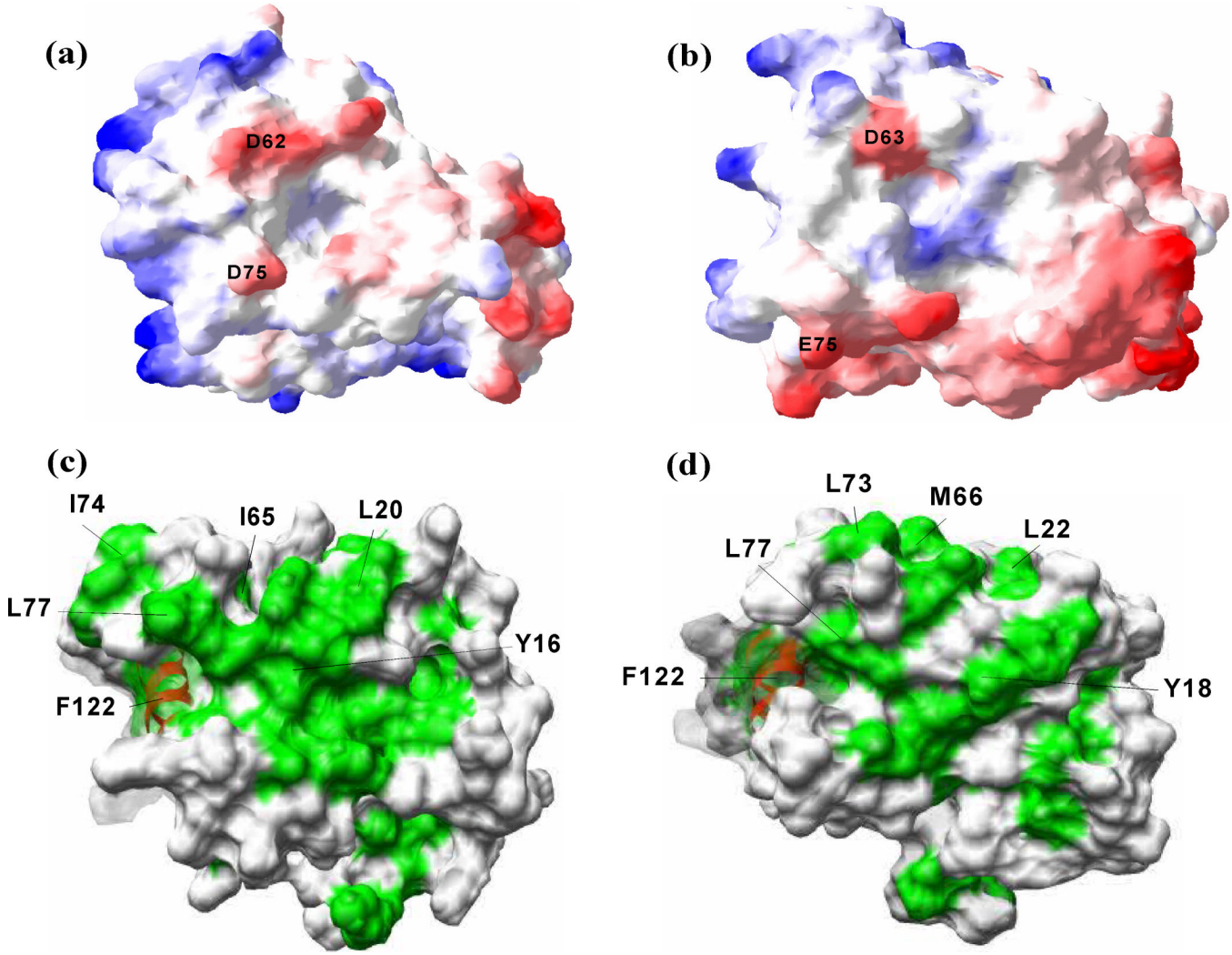

Figure 8.

Comparison of *E. coli* and *Aquifex* NusB proteins. Surface charge representation of (a) AqNusB and (b) EcNusB. Negative charged regions are colored in red while positive charged regions are colored in blue. The surface charge was calculation by Poisson's distribution in SwissPDB viewer[49] at 100 mM salt concentration. The hydrophobic (green) and surfaces are shown for *Aquifex* (c) and *E. coli* (d). Some conserved residues at the binding site are marked in black. The disordered C-terminal residues 142−148 of AqNusB are omitted for clarity.